



A novel investigation into edge effect reduction of 4340 steel spur gear during induction hardening process

Mahyar Parvinzadeh¹ · Sasan Sattarpanah Karganroudi¹ · Narges Omid¹ · Nouredine Barka¹ · Mohamed Khalifa¹

Received: 17 December 2020 / Accepted: 13 January 2021 / Published online: 26 January 2021
© Springer-Verlag London Ltd., part of Springer Nature 2021

Abstract

Induction hardening, a promising approach for selective hardening of metal parts, is widely used for surface hardening, where a hard surface is required alongside a tough core. Regarding the complexity of this process, parts' geometry deeply affects the temperature distribution and hardness profile accordingly. In this study, two magnetic flux concentrators are introduced to our induction machine set in order to control the magnetic flux and consequently hardness profile (case depth) of spur gears. The performance of magnetic flux concentrators is examined by the effect of machine parameters on the case depth and the edge effect of AISI 4340 steel-made spur gear. Design of experiments based on Taguchi method is primarily used to optimize the number of experimental trials. Then, the hardness profiles of heat-treated gears at the tip and root of gears are measured by microindentation hardness tests. The results are analyzed using analysis of variance (ANOVA) and response surface methodology (RSM) to determine the main effect of process parameters, also the best combination of process parameters that maximizes the case depth and minimizes the undesirable feature of edge effect. Finally, the predicted case depth models versus process parameters are developed based on linear regression method. To this end, four predictive models of case depth at tip and root in the edge plane and middle plane of spur gears are generated. Results imply that maximum case depth with minimum edge effect at root and tip is achieved by setting up the highest machine power, longest heating time, and minimum axial gap between concentrators and the spur gear. This study provides a good exploration of case depth in presence of magnetic flux concentrators under various process parameters and gives a reliable guideline towards edge effect during induction hardening process.

Keywords Induction hardening · Spur gear · AISI 4340 steel · ANOVA · RSM · Case hardening

1 Introduction

Induction heating is a complex process that consists of several physical phenomena including thermal, electrical, and magnetic fields. In this process, the heat is generated on the surface of a magnetic object when it is exposed to an altering magnetic field. In fact, eddy currents derived from altering magnetic fields, flow over the object, and inherent electrical resistant of the material leads to heat generation in the object [1]. This method has proven its reliability for being used in mass productions. Induction heating for industrial purposes offers a fast generating of high-intensity heat at a well-defined location in parts with

repeatable quality, low labor cost for operating induction machine, being energy-efficient and ecofriendly. Furthermore, it makes industries capable to treat metallic parts with complex-geometric shapes such as gears and splines. All these advantages lead to delivering fast products with desirable and constant quality and lower cost. Induction heating can be applied to annealing, bonding, brazing, carbide tapping, casting, curing and coating, forging, melting, plastic reflow, heat staking pre-heat and postheat, shrink fitting, and soldering [2]. Besides, this method is widely used for case hardening, which is also known as surface hardening. The case hardening of a spur gear using the induction case hardening process is illustrated in Figure 1 wherein the yellow surface is induction-heated. The machine is equipped with a cooling system, that cools the gear rapidly after heating. This fast cooling increases the generation of martensite phase, in the heated area resulting in a more hardened gear surface compare to the gear core.

Generally, spur gears are subjected to altering forces that are the reason for gears' fatigue failure. Increasing wear-

✉ Sasan Sattarpanah Karganroudi
sasan_sattarpanahkarganroudi@uqar.ca

¹ Department of Mathematics, Computer Science and Engineering, Université du Québec à Rimouski, Rimouski, Québec, Canada

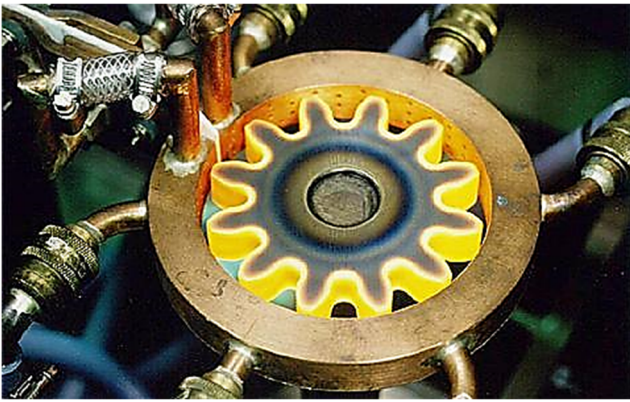


Fig. 1 Induction hardening of a spur gear [3]

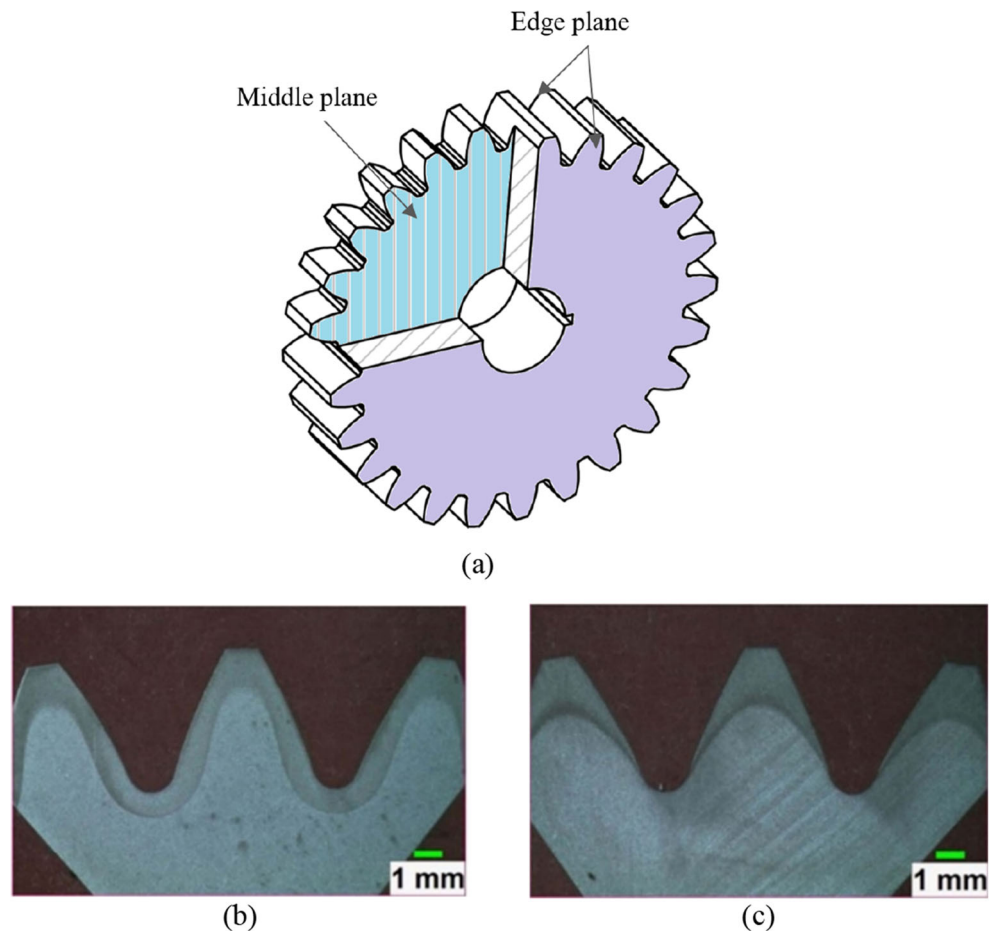
resistant in contact areas resulting in higher contact fatigue strength. One simple solution to this issue is quenching heat treatment, in which the whole part is undergone hardening heat treatment. This increases the martensite phase uniformly in a part, both on the surface and in the core, resulting in a brittle gear, which is not a desirable mechanical property for gears. In this regard, case hardening heat treatment would be a credible choice by providing a fine martensite phase only at the surface layers of the gear. Applying case hardening results in a hard gear surface without changing the hardness and metallurgical microstructure of the gears' core [2, 4]. In general, the result of case hardening highly depends on the components of steel alloys. Overall, steel alloys are categorized by the percentage of constituent alloys into low, medium, and high-alloy steels [5]. In this study, AISI 4340 steel is used, which is low alloy steel presenting the utmost possible toughness and strength in a heat-treated condition, as well as good fatigue resistance. In this study, the purpose of case hardening of AISI 4340 steel gear is to change, to the greatest degree, the perlite and bainite phase to martensite to enhance the surface hardness of gears and to provide fine martensite microstructure. To prevent producing any pearlite or bainite phases during cooling process, the austenite layer should be crystallized uniformly, during heating process [6]. A desirable austenite layer formation could be fulfilled by choosing proper process parameters in induction hardening in which the remaining martensite layer is guaranteed by using a suitable quenching method such as a water shower. Conventional heat treatment procedures for AISI 4340 alloy steel parts is performed by heating the part within a range of 790 to 915 °C (850 °C in our study) to achieve a uniform austenite structure in its surface layer, then a rapid quenching to create maximum possible martensite layer [7–10].

Induction hardening of gears engages with several challenges. The major challenge is in induction heating wherein the edge effect is brought about due to the variable density of magnetic flux at different areas of a part [2, 11]. This variation in flux density causes diverse temperature map through the heated area. Generally, the hardness profile obtained from

hardening methods is not uniform. A typical quenching heat treatment creates a nonuniform martensite layer on the gear surface resulting from a nonuniform metallographic structure through the thickness of the part. In the case of induction hardening of external spur gears with the single-shot method and high-frequency current, the nonuniformity in temperature could be seen in two directions: radial and axial direction. The nonuniformity in axial direction causes a difference of temperature between the root and tip of the gear tooth that is due to the proximity of tooth tips to the induction coil compared to tooth roots. In axial direction, the issue referees to the fact that the generated heat between the middle plane and edge plane of a gear tooth, as shown in Fig. 2a, is not uniform. This is termed “edge effect”, which happens when the current is induced in thin bodies like slabs, stripes, foils, and thin gears in which the thickness of a part is considerably less than its width and length. When eddy currents bend to reverse direction in corners of close areas like gear edges near the end of corners, distortion of current takes place since current tends to break the corners. Overheating or underheating of these specific areas can create an uneven heat profile resulting in a nonuniform martensite layer on the gear [5, 13, 14]. The edge effect of a heat-treated gear using induction heating method is illustrated in Fig. 2b and 2c wherein a different hardness profile between the edge plane of gear tooth (Fig. 2b) and the middle plane of gear tooth (Fig. 2c) can be observed. It is worth mentioning that the most case depth difference between two planes (middle and edge plane) happens at the teeth root of gears.

To the best of the authors' knowledge, there is no technology to eliminate this undesirable effect. However, efforts are done on hindering it as much as possible by utilizing flux concentrators. Process arrangements such as axial and radial gaps (Fig. 4) are of importance in minimizing the edge effect. Therefore, minimizing the edge effect demands optimizing the induction heating machine parameters including machine power, frequency, heating time, and the axial and radial gaps. Over the last few decades researchers attempt to optimize induction heating process parameters with methods such as designing different-shaped coils, using variable power supplies, quenching systems for various part geometries to achieve desirable hardened layer microstructure and case depth. Since the early years of thriving industrial experiences up to now, induction heating technology has seen many improvements such as creating solid-state power supplies instead of motor generator and development of high current, which in their turn have caused more efficient processes with lower costs [2]. Studies are also carried out on the other objectives in the induction hardening field such as finding a relationship between fatigue tooth breakage start point and machine parameter, and case depth using power circulating gear testing machine for steel spur gear [15]. Zhichao et al. [16] investigate the effect of preheating of parts on the residual stress and cracking during quenching of large parts of 4340 steel.

Fig. 2 a Schematic representation of the edge plane and middle plane, and the case depths in b edge plane [12] and c middle plane [12] of a gear



Barglik [17] presented the spatial temperature distribution through a dual frequency induction heated gear and validate the model by experimental studies. Kristoffersen et al. [18] presented research that studies the relationship between residual stress and hardening depth for two microstructures of cylindrical parts by using an X-ray diffraction method. Cajner et al. [19] studied the effects of induction hardening machine parameters on cylindrical workpieces using computer simulation for an electromagnetic process, thermodynamic, microstructural transformations, and hardness distribution in a part. Residual stresses of surface hardened steel parts using induction heating method are also investigated both experimentally, using X-ray diffraction technique, and numerically, using multiphysics finite element modeling [20]. Candeo et al. [21] conducted computer simulations with electromagnetic, thermal, and metallurgical finite element analyses for induction hardening of spur gears. Munikamal et al. [22] exploited ABAQUSTM simulation software to determine the case depth and hardness in surface hardening of automotive steel components such as crankshaft and spur gears. Montalvo et al. [23] used computer simulation to demonstrate the effect of quenching rate on transformation-induced plasticity (TRIP) effect in a high-frequency induction heating process wherein

results showed that the effect is not negligible. Barglik et al. [24] established temperature profiles and the final hardness of a gear wheel using 3D numerical analysis with temperature-dependent parameters of the hardening process. Other research works have also been carried out using 3D simulation to analyze and predict AISI 1045 steel behavior during spot induction hardening (SIH) [25], and to estimate residual stresses in small spur gears hardened by induction heating [26]. Moreover, 3D simulations of multifrequency induction hardening were accomplished for a mathematical model including Maxwell's equations and nonlinear heating equation to eventually link thermal and electromagnetic equations [27]. Computer simulations are also used to determine temperature distribution in a workpiece in multifrequency-induction-hardening with a single coil for parts with complex geometries [28], and to predict material properties for spot continual induction hardening [29]. Recent researches [30–32] are fulfilled to develop numerical studies on dual-frequency hardening process of AISI 300 M gear. They introduce a mathematical model of the process with the help of time-temperature-austenitization (TTA) and continuous-cooling-temperature (CCT) diagrams [33]. Marco Baldan et al, investigated the induction heating process from another point of view, wherein

multifidelity optimization approach is implemented to reduce process time [34]. Li et al. [16] also tried to optimize the induction heating temperature of 55CrMo Steel ball screws in which they used the martensite fraction value as main criterion of their study. The outcome of the study shows that the more temperature, the more hardness and the more martensite volume fraction generation [35].

To investigate the effects of heat treatment process parameters on pipes residual stress in medium-frequency induction, 3D analysis of medium-frequency induction heating of steel pipes are conducted [36]. More recently, Xiaobin et al. [37] carried out numerical and experimental studies on local induction heating of large-diameter gear rolling. It is worth noting that Tong et al. [38] applied a couple of simulations and numerical models together to investigate residual stress distributions of gear tooth in an asynchronous dual-frequency (ADF) induction hardening process for spur gears. Our research group implemented new techniques to accomplish enhancement in the surface hardening of gears. We used a 3D model simulation of spur gears to the determinate extensive effect of machine parameters and coil geometry on the final temperature distribution on specimens [39]. The most effective machine parameters on the case depth of spur gears [40] and the effects of machine parameters on the case depth of flat cylinders by using computational simulation [5] were studied. More recently, we studied the effect of flux concentrators on the case depth of gears using experiments, analytics, and simulation software to achieve a more efficient method. In this regard, we investigated using COMSOLTM simulation for a 3D finite element model on spur gears [5]. We further evaluated the effects of flux concentrators on the edge effect of gear tooth [12]. Researches studying the effect of flux concentrators on the final temperature distribution and case depth in the induction heating of spur gears using finite element analysis, analysis of variance (ANOVA), and artificial neural network methods, are also conducted to predict models leading to the edge effect reduction [41, 42].

Although preceding researches have investigated the case depth of simple and symmetrical shapes, edge effect control in complex shapes such as gears is still a challenge. To the best of the authors' knowledge, no study analyzes and prioritizes the influence of induction machine parameters on the case depth of spur gears in both experimental approach and statistical analyses. In this research, an experimental method is adopted, and results are explored using ANOVA to analyze the effect of induction surface heating parameters on the case depth. This statistic approach is planned, to perform most precisely yet with the optimum number of tests. This proposed statistical approach is developed in progressive steps. The first step is to prepare an experimental plan according to Taguchi planning method [43]. The second step is involved in defining the induction hardening ranges for spur gears. The third step is consisted of acquiring the experimental results and analyzing

the data using ANOVA [44]. Based on ANOVA analyses and linear regressions, predictive models are developed to assess the case depth in the tip and root of gear teeth. This model is executed to achieve an optimized condition in the induction heating process for the case depth of spur gears. The effect of flux concentrators on edge effect and the consequences of using them in induction heating of thin spur gears are also investigated in this study. The feasibility and effectiveness of the proposed approach led to an accurate and reliable statistical model for predicting the case depth of spur gears. This article is formed as follows: Section 2 presents the methodology of our experimental tests based on induction surface heating and its related parameters. Results of experimentation, statistical and sensitivity analyses, and edge effect discussions are then reported in Section 3. In the end, Section 4 presents conclusions and ideas for future works in this field.

2 Experiment procedure

2.1 Materials and induction heating process

The induction heating experiments in this study have been performed on spur gears made of AISI 4340 steel, that are used widely in power transmission gears due to high strength in heat-treated condition and excellent fatigue strength. The chemical composition of AISI 4340 steel and its mechanical characteristics are presented in Tables 1 and 2 respectively.

Induction hardening tests were carried out by the induction machine illustrated in Fig. 3. The machine exploits two generators to produce a varying range of frequencies from medium to high frequency. The frequency rate is controlled by generator power in a way that the maximum frequency will be achieved by the machine's maximum power, which in its turn is obtained by combining the maximum power of two generators. In order to reach the maximum frequency, first, the audio-frequency of 10 kHz is obtained at the maximum generator power of 550 KW using solid-state converters. Then, 200 kHz frequency is generated by a radiofrequency (RF) transistor generator at the maximum power of the second generator in 450 kW. In this study, the radiofrequency (RF) transistor generator operates at 200 kHz. The real-time monitoring (RTM) module is also applied to ensure the quality of the process in a way that the parameters are checked whether the actual parameters are the same as the operator's intended parameters.

The schematic of a spur gear and flux concentrators is illustrated in Fig. 4. Two flux concentrators are gears exactly similar to the master spur gear. They have positioned above and under the spur gear employing an available stand kit and using AISI 1010 steel shims to ensure axial gaps. The thickness and the outer diameter of these shims are 0.2 ± 0.05 mm and 31.75 mm respectively. The master spur gear is

Table 1 AISI 4340 steel chemical composition in wt% [45]

| Element | Ni | Cr | Mn | C | Mo | Si | S | P |
|-------------|-----------|-----------|-----------|-----------|-----------|-----------|------|-------|
| Content (%) | 1.65–2.00 | 0.70–0.90 | 0.60–0.80 | 0.38–0.43 | 0.20–0.30 | 0.15–0.30 | 0.04 | 0.035 |

surrounded by a coil with 140 mm of outer diameter, 110 mm of inner diameter, a useful section of 7×7 mm, and 2 mm thickness. Finally, the machine is equipped with a cooling system comprising a jet of coolant solution containing 92% water and 8% polymers. The quenching heat treatment is performed by a cooling system which is situated under the gears as shown in Fig. 3.

All used gears in this research are made of AISI 4340 steel with identical shape and geometry with an outer diameter of 104.3 mm, and a thickness of 6.5 mm. To make sure that gears are containing homogenous mechanical and microstructural properties, the gears were undergone quenching and tempering heat treatments. Using microhardness tests the uniform hardness of gears reaches approximately 40 HRC in this step. It should be noted that due to the geometrical complexity of gears, the roots and tips of gear teeth are exposed to different magnetic flux densities. To prevent overheating, the temperature should not exceed the austenite transformation temperature. As already mentioned, induction heating of gears is a function of the process parameters. To avoid redundancy and to find an optimum number of parameter variations for experimental tests, a design of experiment method is implemented. The efficiency and simplicity of factorial design and more specifically Taguchi planning method, make it the most commonly used method allowing choosing factor levels and simultaneous mode of factor variations, studying the effect of each factor on the process [43, 48]. To predict experimentally the case depth in tip and root of spur gears, Taguchi method is used to minimize the number of our tests while providing expressive results for statistic analyses.

2.2 Design of experiments based on Taguchi method

The generated heat is adjustable by machine input variables consisting of machine power, heating time, and frequency. However, modifying frequency in induction heating is not as straightforward as machine power and heating time. The concentrator gap also plays an important role in controlling the

induction heating of gears. The axial and radial gaps, the most important geometrical factors of the process, are determined as a gap between the gear and coil as well as the gear and concentrator respectively (Fig. 4). In this research, the axial gap is considered as a study term while the radial gap is preserved as a constant at 2.3 mm. In this regard, researches on the variation of radial gap and its effect could be the subject of investigation in further studies. Regarding Taguchi method, three (3) levels for each parameter are considered to cover all practical parameter ranges including low, medium, and high levels which is presented in Table 3. The controlling parameters are power (P), heating time (T), and the gap between a concentrator and the master gear (G).

As already mentioned, to develop a reliable analytical model through analysis of induction heat treatment experiments, it is essential to carry out a properly designed test plan to perform a minimum efficient number of experimentations using Taguchi experiment planning. The suitable range of factors along with the Taguchi experimental design makes the process more robust, efficient, and with a more consistent performance in a minimal number of trials [49, 50]. In the case of induction hardening processes, it is important to search for the variation of experimental parameters allowing minimal and maximal case depth transformation. To this end, the maximal and minimal parameter range tuning is necessary before establishing parameter levels. This is defined during our preliminary tests as mentioned before in this section. Based on Taguchi planning method, the design of experiments that addresses this experiment is an L_9 orthogonal matrix corresponding to nine (9) tests. Consequently, each test consists of a unique combination of parameter levels which are shown in Table 4.

2.3 Case depth measurement

In order to measure the case depth of gear after the case hardening process, microindentation tests using Clemex microhardness [51] testing machine is performed on the edge and

Table 2 Mechanical properties of AISI 4340 steel Q and T [46]

| Yield strength [MPa] | Ultimate tensile strength [MPa] | Elongation at break [%] | Hardness Rockwell C [HRC] |
|----------------------|---------------------------------|-------------------------|---------------------------|
| 847 | 1020 | 20.6 | 34 |

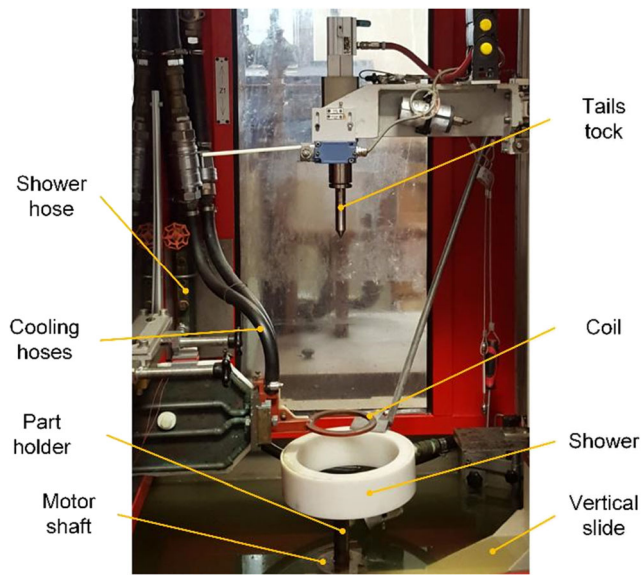


Fig. 3 Induction machine and operation system [47]

middle planes of gears (Fig. 2a). Microindentation tests are repeated on each of nine induction heated gear to evaluate the effect of process parameters on case hardening. These results are shown in Table 5 which presents the case depth measurement at gears tooth root in the middle plane (d_{RM}) and the edge plane (d_{RE}) as well as at gears tooth tip in the middle plane (d_{TM}) and the edge plane (d_{TE}).

It can be observed in Table 5 that increasing P and T may result in reducing d_R ; however, no significant effect could be seen for d_T . These results imply that the maximum and minimum case depth occurs in tests 3 and 1 respectively. The hardness profile of the gear on tip and root area resulting from tests 1 and 3 are compared in Figs. 5 and 6. Three regions could be noticed in these graphs: the first region presents a

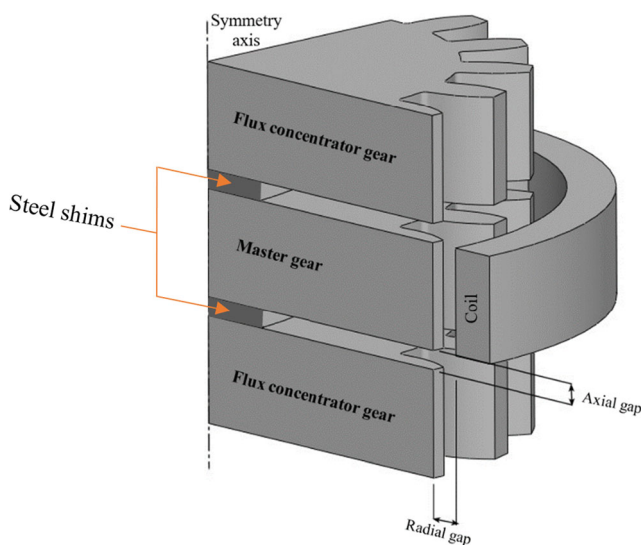


Fig. 4 Schematic presentation of the model's geometry

Table 3 Experimental factors and range of variables for each level applied to Taguchi method

| Parameter | Unit | Abbreviation | Level 1 | Level 2 | Level 3 |
|-----------|------|--------------|---------|---------|---------|
| Power | kW | P | 143.0 | 156.5 | 170.0 |
| Time | s | T | 0.45 | 0.50 | 0.55 |
| Gap | mm | G | 0.20 | 0.60 | 1.00 |

hardened surface layer due to martensitic microstructure formation, the second region displays a hardness drop to approximately the core material hardness, and the third region preserves the initial hardness of gear as it did not receive the thermal flow [52]. Figure 5a demonstrates the maximum and minimum obtained case depth at middle-root (d_{RM}) resulted respectively from test 3 and test 1. Figure 5b shows the maximum and minimum case depth at edge-root (d_{RE}). In Fig. 6a, the maximum and the minimum attained case depths at middle-tip (d_{TM}) of test 1 and test 3 are compared together. Moreover, the comparison between the maximum and minimum case depth at edge-tip (d_{TE}) is presented in Fig. 6b.

Three main conclusions can be drawn from Table 5. First, the maximum case depth for both root and tip can be achieved at the highest machine power and the longest heating time that are 170.0 kW and 0.55 s respectively. In contrast, the minimum case depth can be carried out at the lowest level of parameters (143.0 kW and 0.45 s). This is due to the fact that the more heating time, lets the heat to convey through more surface, resulting in a more heated area. Second, in each gear, generally, the case depths in the middle plane are deeper than the case depth in the edge plane. This is an affirmation of generating more current density at the middle of teeth compared to the edges due to the induction edge effect. Third, a proper variation of collected case depths in terms of having fine coverage between the maximum and minimum depths in roots and tips, remarks on the credibility of well-designed tests with Taguchi method.

Table 4 Design of experiences, L_9 orthogonal matrix, and experimental results

| Tests no. | P [kW] | T [s] | G [mm] |
|-----------|--------|-------|--------|
| 1 | 143.0 | 0.45 | 0.2 |
| 2 | 156.5 | 0.50 | 0.2 |
| 3 | 170.0 | 0.55 | 0.2 |
| 4 | 143.0 | 0.50 | 0.6 |
| 5 | 156.5 | 0.55 | 0.6 |
| 6 | 170.0 | 0.45 | 0.6 |
| 7 | 143.0 | 0.55 | 1.0 |
| 8 | 156.5 | 0.45 | 1.0 |
| 9 | 170.0 | 0.50 | 1.0 |

Table 5 Microhardness test results of the tooth root (R) and tooth tip (T); hardness has been measured on the middle plane (M) and the edge plane (E)

| Test no. | Parameters | | | Root | | Tip | |
|----------|------------|-------|--------|---------------|---------------|---------------|---------------|
| | P [kW] | T [s] | G [mm] | d_{RM} [mm] | d_{RE} [mm] | d_{TM} [mm] | d_{TE} [mm] |
| 1 | 143.0 | 0.45 | 0.2 | 0.35 | 0.10 | 2.45 | 2.20 |
| 2 | 156.5 | 0.50 | 0.2 | 0.50 | 0.40 | 3.35 | 2.90 |
| 3 | 170.0 | 0.55 | 0.2 | 0.60 | 0.65 | 3.95 | 3.70 |
| 4 | 143.0 | 0.50 | 0.6 | 0.45 | 0.20 | 2.90 | 2.30 |
| 5 | 156.5 | 0.55 | 0.6 | 0.55 | 0.50 | 3.60 | 3.10 |
| 6 | 170.0 | 0.45 | 0.6 | 0.50 | 0.45 | 3.50 | 2.65 |
| 7 | 143.0 | 0.55 | 1.0 | 0.55 | 0.50 | 3.60 | 2.80 |
| 8 | 156.5 | 0.45 | 1.0 | 0.55 | 0.40 | 3.20 | 2.20 |
| 9 | 170.0 | 0.50 | 1.0 | 0.60 | 0.60 | 3.90 | 3.25 |

3 Effect of parameters on hardness profile

3.1 Statistical analysis and parameters contribution

To investigate the effect and influence of each parameter on the case depth of spur gears, analyses of variance (ANOVA) are applied [53, 54]. The exactitude of the regression model is evaluated by an *F* test based on ANOVA. General systematic details are presented in Tables 6, 7, 8, and 9. Terms that present the results of the analyses are degrees of freedom (DoF), sum of squares, contribution percentage, *F* value, and *P* value [53, 55]. To determine whether the effect of process parameters on the case depth is statistically significant, ANOVA calculates *p* value based on *F* test. Comparing *p* value with the designated significance level (α) determines whether the null hypothesis can be rejected or not. The null hypothesis, in this case, states that the effect of studied parameters is not significant on the case depth. We reject the null hypothesis when the calculated *p* value is less than the designated significance

level. In this study, we use a significance level (α) of 0.05 which indicates that there is a 5% risk of concluding that a parameter has a significant effect on the process when there is no actual effect.

In this study, linear regression is developed based on ANOVA results wherein the case depths are estimated as a dependent variable (d_{RE} , d_{RM} , d_{TE} , and d_{TM}), and power (*P*), heating time (*T*), and concentrator’s gap (*G*) as independent variables. Preliminary effect analyses for each of the dependent variables (d_{RE} , d_{RM} , d_{TE} , d_{TM}), using interaction diagrams of factors in three levels, show that there are no significant interactions between independent variables. In this regard, adding factor interactions into ANOVA model can use the DoF up, and make the model complicated and incalculable [56]. During preliminary ANOVA analyses, first-order interaction of factors (*T*×*P*, *T*×*G*, and *P*×*G*) are added to the ANOVA model along with the factors (*P*, *T*, and *G*) to determine the significance of their effect on d_{RM} , d_{RE} , d_{TE} , and d_{TM} . These results showed that the calculated *p* value for

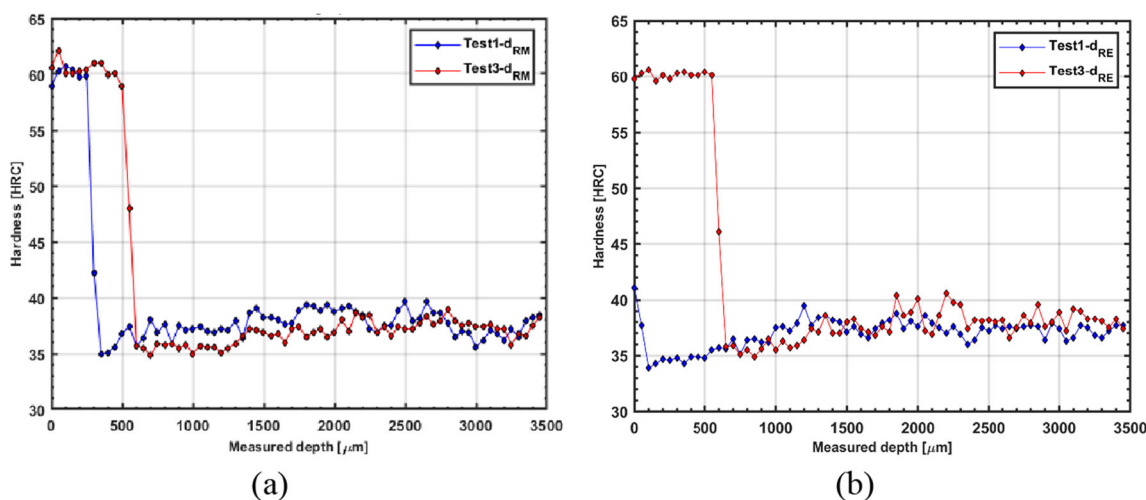


Fig. 5 Microhardness of teeth root for test 1 and test 3 (a) in middle plane d_{RM} (b) in edge plane d_{RE}

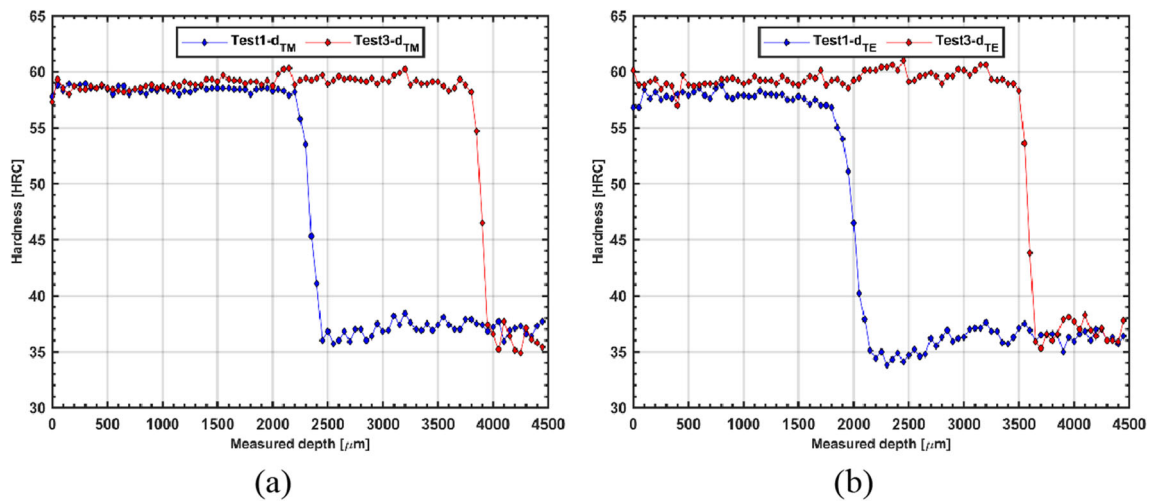


Fig. 6 Microhardness of teeth tip for test 1 and test 3 (a) in middle plane d_{TM} (b) in edge plane d_{TE}

interactions was much higher than the significance level (0.05), which infers that the interactions are not significant in these cases. These large p values raise a red flag for an overfitted model which can consequently lead to erroneous predictive models [57]. For this reason and to provide a reliable goodness-of-fit regression model, ANOVA analyses for d_{RM} , d_{RE} , d_{TE} , and d_{TM} are performed without the interaction of independent factors.

Table 6 shows ANOVA analyses for d_{RM} in which the p value for P, G, and T are respectively 0.004, 0.008, and 0.017. These p values are less than 0.05, hence, the null hypothesis of nonsignificant factors for these terms is rejected. It can be observed that machine power (P) is the most effective parameter, then heating time (T), and finally concentrator’s gap (G) with respect to their incremental quantity of p values. Thinking back to p values for d_{RM} and considering the contribution percentage variables, it can be concluded that P is the most effective term in d_{RM} . In the same way, for d_{RE} in Table 7, P and T respectively are the most effective parameters. Considering contribution percentage of 53.88% and p value of 0.001 for d_{RE} declares that P is the most effective term in d_{RE} .

Table 8 for d_{TM} remarks p value of 0.000 for P and 0.001 for T. p value of 0.000 for P implies that the null hypothesis is

rejected with high confidence. Considering a contribution of 52.32%, the effect of P in d_{TM} is very significant. p value of 0.001 and the contribution of 36.33% for T shows also the significant effect of this parameter. Results in Table 9 expresses that in d_{TE} , the p value of T is 0.000, and of P is 0.001. This indicates that T is the primary effective parameter and P is the secondary effective term in d_{TE} . It should be noted that the effect of G was not significant enough to be considered as a contributing factor, and this factor is eliminated during iterations of ANOVA.

3.2 The main effect of process parameters

For easier correlation determination between dependent and independent variables, statistical methods are used to specify the effect trend of each parameter on the response. Using the sum of squares calculated for each parameter in ANOVA tables, the contribution of each factor in the total sum of squares indicates the effect of parameter values on the response variation. To this end, the results of ANOVA analysis are used to determine the contribution ratio of each parameter (P, T, and G) in the case depths for root (d_{RE} , and d_{RM}) and tip (d_{TE} , and d_{TM}) of the gear. As shown in Tables 6, 7, 8, and 9, the contribution percentage of each process parameter (P, T,

Table 6 Results of ANOVA for micro-hardness tests at root and on middle plane (d_{RM}) of gear

| Factors | DoF | Sum of squares | Contribution (%) | F value | P value |
|---------|-----|----------------|------------------|---------|---------|
| P | 1 | 0.020417 | 40.83 | 24.50 | 0.004 |
| T | 1 | 0.015000 | 30.00 | 18.00 | 0.008 |
| G | 1 | 0.010417 | 20.83 | 12.50 | 0.017 |
| Error | 5 | 0.004167 | 8.34 | | |
| Total | 8 | 0.050000 | 100.00 | | |

Table 7 Results of ANOVA for micro-hardness tests at root and on edge plane (d_{RE}) of gear

| Factors | DoF | Sum of squares | Contribution | F value | P value |
|---------|-----|----------------|--------------|---------|---------|
| P | 1 | 0.13500 | 53.88% | 50.10 | 0.001 |
| T | 1 | 0.08167 | 32.59% | 30.31 | 0.003 |
| G | 1 | 0.02042 | 8.15% | 7.58 | 0.040 |
| Error | 5 | 0.01347 | 5.38% | | |
| Total | 8 | 0.25056 | 100.00% | | |

Table 8 Results of ANOVA for microhardness tests at tip and on middle plane (d_{TM}) of gear

| Factors | DoF | Sum of squares | Contribution | F value | P value |
|---------|-----|----------------|--------------|---------|---------|
| P | 1 | 0.96000 | 52.32% | 82.88 | 0.000 |
| T | 1 | 0.66667 | 36.33% | 57.55 | 0.001 |
| G | 1 | 0.15042 | 8.20% | 12.99 | 0.015 |
| Error | 5 | 0.05792 | 3.15% | | |
| Total | 8 | 1.83500 | 100.00% | | |

and G) confirms in most cases, that the highest contribution percentages belong to the parameters P and T, while G has a minimum influence on the case depth. The contribution percentages of P are 40.83%, 53.88%, 52.32%, and 41.91%, and of T are 30.00%, 32.59%, 36.33%, and 51.51% for d_{RM} , d_{RE} , d_{TM} , and d_{TE} in turn. These contribution percentages concerning G are 20.83%, 8.15%, and 8.20%, for d_{RM} , d_{RE} , and d_{TM} respectively.

In order to have a better visual perspective of the impact of each parameter on responses, the main effect plots are drawn in MATLABTM, in which the statistical mean value of responses in each level of parameters presents the trend of each parameter on the response. In this regard, the steeper is the plot, the more influencing is the studied parameter. The main plots present separately the effectiveness of each parameter at varying levels. Through these plots, each level of P, T, and G are linked to their response mean value at the parameter level. Hence, to examine differences between level means of independent variables (P, T, G) on each of four responses (d_{RE} , d_{RM} , d_{TE} , and d_{TM}), main effect plots are presented in Fig. 7a and b.

Figure 7a is dedicated to show the case depths of tooth root where d_{RM} and d_{RE} are respectively distinct by red and blue lines. Generally, the steepness of lines from a level to the next level shows the effect of each parameter on the case depth response; the steeper the line, the more effective the parameter on case depths. It could be observed in Fig. 7a, for d_{RM} with red lines, that P and T are the most effective parameters over the three levels due to the biggest range of the case depth from the first to the third level. From the first to the second level, P shows the largest effect, which is also the most significant effect. However, from the second level to the third, G shows

Table 9 Results of ANOVA for microhardness tests at tip and on edge plane (d_{TE}) of gear

| Factors | DoF | Sum of squares | Contribution | F value | P value |
|---------|-----|----------------|--------------|---------|---------|
| P | 1 | 0.8817 | 41.91% | 38.20 | 0.001 |
| T | 1 | 1.0837 | 51.51% | 46.96 | 0.000 |
| Error | 6 | 0.1385 | 6.58% | | |
| Total | 8 | 2.1039 | 100.00% | | |

more contribution. It means the considerable effect of G on the case depth happens at the higher values of G. Overall, regarding the case depth changes, P is the most effective parameter and the next important parameters are T and G with close effects on d_{RM} . Blue lines in Fig. 7a expose a dominant influence of P compare to T and G, because of a steeper line of P over the three levels. Case depth changes over the three levels are more vivid in the edge plane wherein P and T mainly affect the case depth, then G with a considerable difference. It worth mentioning that G plays the same role as in the middle plane; very low effect from the first to the second level (the representative line for this part is almost flat) and steeper from the second to the third level.

Step red lines of d_{TM} , presented in Fig. 7b, emphasize the most influential rule of P and T on d_{TM} . Almost the same length and steep line and the same starting and finishing point of P and T in their levels approve this deduction. This is while the influence of G on d_{TM} is not comparable to P and T. Blue representative lines of d_{TE} show that the effect of T is the most in all three levels while P is also considered as having the main effect on the case depth. In contrast, G has a minor effect compared to P and T.

3.3 Predictive models based on linear regression

To explain a mathematical relationship between the dependent and independent variables in a predictive model, regression equations based on minimizing mean squared errors, are exerted. The regression equations estimate responses (d_{RM} , d_{RE} , d_{TM} , and d_{TE}) depending on the parameters of this study (P, T, and G). As presented in section 3.1, the highly effective parameters concerning each response are analyzed by ANOVA and presented in Tables 6, 7, 8, and 9. The regression equations based on these analyzed parameters are presented for d_{RM} , d_{RE} , d_{TM} , and d_{TE} respectively in Eqs. 1 to 4.

$$d_{RM} = -0.722 + 0.1042 \times G + 0.004321 \times P + 1.000 \times T \quad (1)$$

$$d_{RE} = -2.572 + 0.1458 \times G + 0.01111 \times P + 2.333 \times T \quad (2)$$

$$d_{TM} = -4.825 + 0.396 \times G + 0.02963 \times P + 6.667 \times T \quad (3)$$

$$d_{TE} = -5.905 + 0.02840 \times P + 8.05 \times T \quad (4)$$

The coefficient (denoted by R^2 or R-squared) is an indicator to evaluate the precision of regression models. The R^2 assesses the reliability of regression equations in the range of test variation. The R^2 for Eq. 1 is calculated 91.67%, which declares that the equation can predict 91.67% of the variation case depth in d_{RM} . The R^2 for predictive equations of d_{RE} , d_{TM} , and d_{TE} (Eq. 2 to 3) are 94.62%, 96.84%, and 93.42% respectively. These R^2 values show that the regression equations are well fitted to experimental results. The graphical presentations of these predictive models (predicted), experiment results (measured), and the difference between (residual)

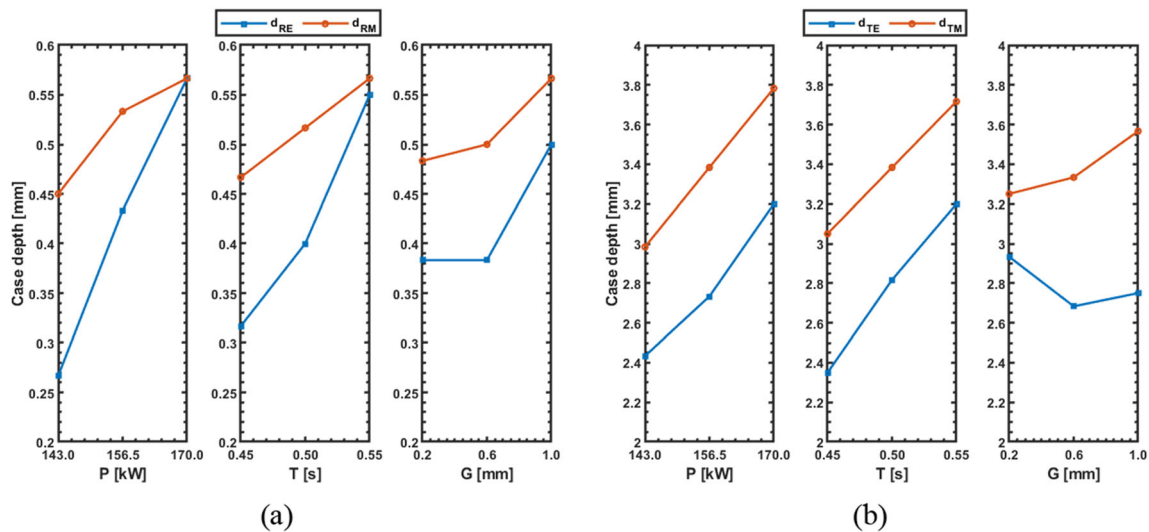


Fig. 7 Main effect plots of case depth on middle and edge planes at a root b tip

versus case depths (d_{RM} , d_{RE} , d_{TM} , and d_{TE}) are demonstrated in Figs. 8 and 9. These curves present a visual comparison between predictive model and experimentation results. To evaluate quantitatively the preciseness of predictive models, for each of the four responses (d_{RM} , d_{RE} , d_{TM} , and d_{TE}), obtained case depths of models are compared to their experimentation outcomes. To this end, Eq. 5 is utilized to quantify statistically the error percentage of models.

$$\text{Error (\%)} = \frac{|\text{Predicted} - \text{Measured}|}{\text{Measured}} \times 100 \quad (5)$$

The average estimated errors for the response models (d_{RM} , d_{RE} , d_{TM} , and d_{TE}) are respectively 3.65%, 9.54%, 2.00%, and 8.03%. Results imply that case depths d_{RM} , d_{RE} , d_{TM} , and d_{TE} are computed with a good accuracy wherein the average estimation errors are less than 10%.

3.4 Response surfaces and sensitivity analysis

To investigate the trend of predictive response models (d_{RM} , d_{RE} , d_{TM} , and d_{TE}) with respect to their most effective terms, contour plots are drawn in Figs. 10 and 11 using MATLABTM. Contour plots are color-based maps drawn through two independent variables, presented on vertical and horizontal axes, displaying the variation a response by color gradient and isolines. These plots are useful when the objective is to specify which level combinations of parameters optimize the response. considering that the most important factors in our experimental responses are machine power (P) and heating time (T), the trend of case depth versus the variation of these parameters are presented in this study. The contour plot of d_{RM} is presented in Fig. 10a where a linear relationship between machine power and heating time versus case depth is illustrated, which represents graphically Eq. 1 for d_{RM} . It

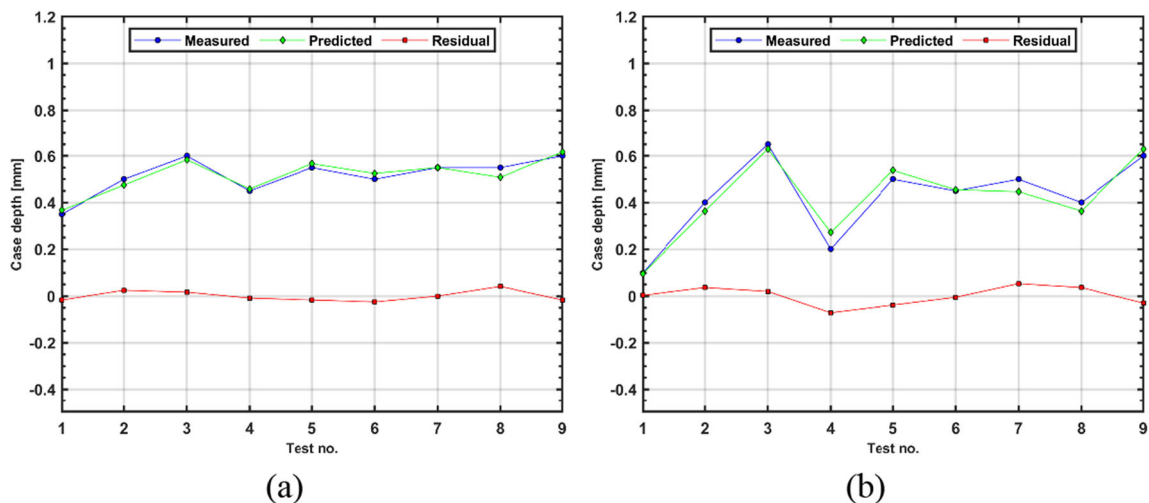


Fig. 8 Case depth measured by experiments, predicted by regression equations and their residuals in a d_{RM} b d_{RE}

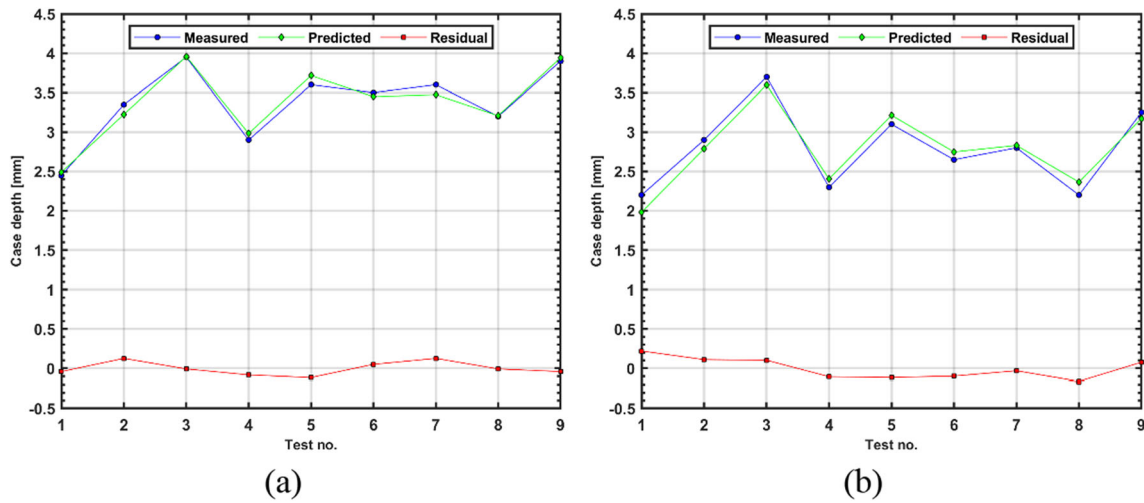


Fig. 9 Case depth measured by experiments, predicted by regression equations and their residuals in **a** d_{TM} **b** d_{TE}

can be inferred from this plot that increasing P and T results in a deeper case depth in middle plane at tooth root of gear. In this regard, the maximum case depth can be obtained at the highest level of P and T . In Fig. 10b, the linear relation between independent variables (P and T) and response (d_{RE}) is found similar to that of d_{RM} . Increasing P and T leads to increasing the case depth. Thus, the highest case depth in d_{RE} is also obtainable with the highest level of P and T .

Figure 11a presents the contour plot of P and T versus the case depth at gears' tooth in its middle plane. It demonstrates more intense effects of P and T on case depth compare to their effect at the gear's root, which is due to the proximity of tooth tip to the coil. This is concluded from a comparison of the highest d_{TM} (3.8) which is shown in yellow color in Fig. 11a. The effects of changing P and T on d_{TE} are displayed in Fig. 11b in which d_{TE} raises with increasing P and T . Highest d_{TE} could be achieved at the highest P and T . It is worth noting that the

maximum case depth of d_{TE} is slightly less than d_{TM} in the range of our experimentations. The general conclusion in this section is that the case depth increases with the increase of P and T .

3.5 Edge effect discussion

The more radial distance of the coil from tip of gear results in a nonuniform case depth (as previously shown in Fig. 2c), where the case depth on the tip is more pronounced compared with the root of gear teeth. Referring to previous studies, induced eddy currents affect the case depth profile causing overheating of some areas, depending on the geometry of part which is exposed to induction heating. This leads to a case depth profile in edge plane that is different from the one in middle plane. The main purpose of this study is to investigate, analytically and experimentally, the machine parameters in order to minimize the edge effect, case depth difference in

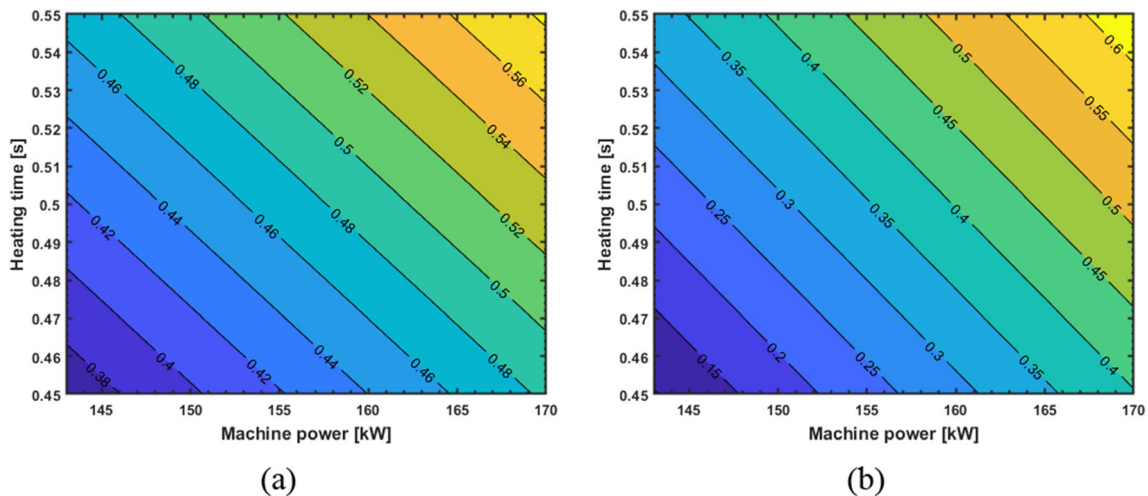


Fig. 10 Contour plots of P and T versus case depths at gear's root in **a** middle plane (d_{RM}) **b** edge plane (d_{RE})

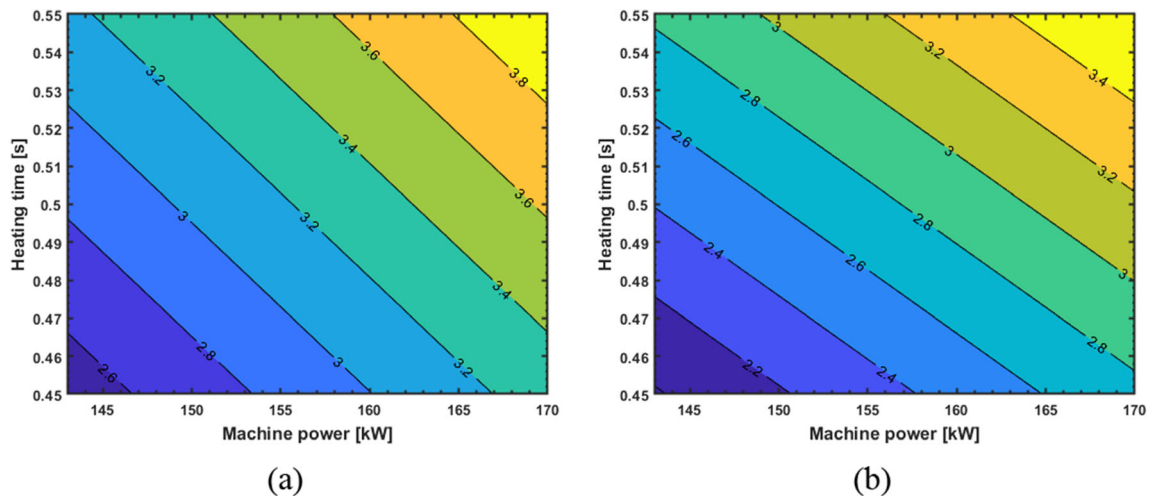


Fig. 11 Contour plots of P and T versus case depths at gear's tip in **a** middle plane (d_{TM}), **b** edge plane (d_{TE})

edge plane (d_{RE} and d_{RM}) over middle plane (d_{TE} and d_{TM}), using flux concentrators. To this end, the less case depth differences between middle and edge planes consider as a more ideal case depth profile in spur gears. Studying the effect of machine parameters on the case depth profile, monitoring it separately in middle and edge planes, it is concluded that increasing P and T results in a deeper case depth. Although reaching deeper case depth fulfills our goal to reach maximum induction heating performance, an ideal case depth profile is the one with the least edge effect. To measure the edge effect quantitatively, we introduce edge effect indicators of gears tooth at root, the difference of case depths measured in middle plain and edge of tooth root (Δ_{dR}), and tip, the difference of case depths measured in middle plain and edge of tooth tip (Δ_{dT}). The case depth difference between middle and edge planes at root and tip is shown in Fig. 12.

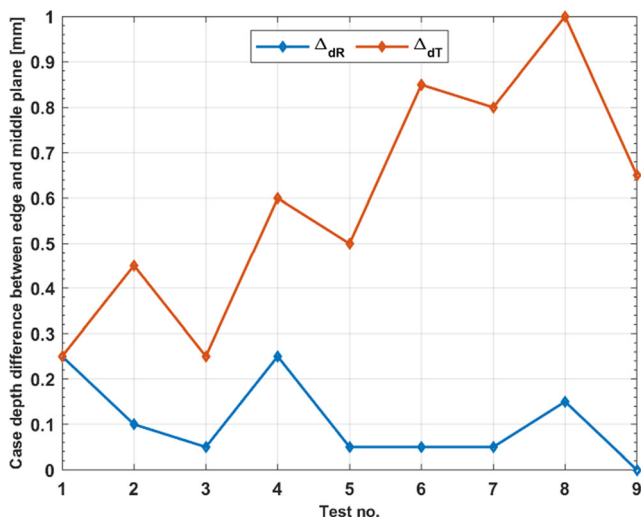


Fig. 12 Edge effect comparison of experimental tests at root (Δ_{dR}) and tip (Δ_{dT}) of gears' tooth

The red line in Fig. 12 represents edge effect at tip of gears tooth. It shows a general enhancement in edge effect at tooth tip with respect to tests from 1 to 9. However, the increasing trend is not uniform, and a considerable reduction in edge effect happens in tests 3, 5, 7, and 9. This is because of an increase of both T and P in these tests compared to the others with an exception for test number 7 that a significant enhancement in T (0.1 s) compensate for P reduction from 170 to 143 kW. The minimum edge effect, and consequently the best case profiles at tip are achieved in tests number 1 and 3, where parameters P and T are at their minimum and maximum level respectively; 143 kW and 0.45 s for test number 1, and 170 kW and 0.55 s for test number 3. It should be mentioned that the effect of G is negligible compare to T and P due to their higher contribution percentage (Tables 8 and 9).

The blue line in Fig. 12 represents the edge effect at root of gears' tooth. It shows a different trend compared to the edge effect at tip. The edge effect is less pronounced in tooth root compare to the tip since the case depth is generally less than tip due to its proximity to the induction coil. In this regard, the effect of G is not negligible at root (the contribution effect of G is 20.83% in middle plane and 8.15% in edge plane). From tests 1 to 9, G increased from 0.2 to 1 mm which shows a general decreasing trend in edge effect. The minimum edge effects happen at test numbers 3, 5, 6, and 9. However, test number 3 is the one in which the edge effect is minimum for both tip and root and provides higher case depth. Therefore, we can conclude that the optimum case depth profile is obtainable in test 3 wherein P and T are at their maximum level, 170 kW, and 0.55 s respectively.

4 Conclusions

In this article, 4340 steel-made spur gears are used to investigate the effects of induction heating process

parameters namely machine power, axial gap between flux concentrators and the master gear, and heating time as independent variables (inputs) on the edge effect. The case depth is measured in four different areas on each gear: at tip and root of gears in edge plane and middle plane. Using Taguchi method, nine experiments are designed to combine four mentioned process parameters in three levels each. Measuring the case depths, the results are statically studied by analyses of variance (ANOVA). The predicted regression model of case depth in four areas of gears, at gear tips (d_{TM} and d_{TE}) and roots (d_{RM} , d_{RE}) are developed. The main effect plots, regression equations, error residuals, and contour plots of each response are developed and analyzed in this study. The results indicate that the total accuracy of predictive models is fine since the average errors of models are in an acceptable range: 3.65%, 9.54%, 2.00%, and 8.03% for d_{RM} , d_{RE} , d_{TM} , and d_{TE} respectively. Results demonstrate that power and heating time are the dominant parameters in case depth. The contribution percentage of machine power are 40.83%, 53.88%, 52.32%, and 41.91%, and of heating time are 30.00%, 32.59%, 36.33%, and 51.51% for d_{RM} , d_{RE} , d_{TM} , and d_{TE} in turn. Generally, the axial gap does not show a significant effect on the case depth. It does not affect the case depth in low levels, while it shows moderate effects in higher levels of the gap. The overall conclusion determines that case depth profile in middle plane is controllable via machine parameters, and the best-exploited range of parameters can maximize case depth while minimizing edge effect. The highest machine power and longest heating time in conjunction with the smallest axial gap contribute to an optimized case depth.

Although the results of this study are promising, some improvements and applications can be foreseen. As already mentioned, this work can be improved by taking into consideration the effect of the radial gap of flux concentrators concerning the case depth of induction-heated gears. To optimize surface treatment of the other parts like discs, bevel gears, and helical gears which have different shapes than spur gears, experimental test benches as well as predictive models can be developed. In this regard, applying artificial intelligence to create and enhance the models on helical gear could be the next project to perform.

Authors' contributions The authors' contributions are as follows: Nouredine Barka and Mohamed Khalifa conceived, planned, and carried out the experiments; Mahyar Parvinezadeh, Sasan Sattarpanah Karganroudi, and Narges Omid contributed to the interpretation of the results. Sasan Sattarpanah Karganroudi took the lead in writing the manuscript; Mahyar Parvinezadeh, and Narges Omid contributed actively in writing the manuscript; all authors provided critical feedback and helped shape the research, analysis and manuscript.

Data availability All data used in this paper are available.

Declarations

Ethics approval This article does not involve human or animal participation or data, therefore ethics approval is not applicable.

Consent to participate This article does not involve human or animal participation or data, therefore consent to participate is not applicable.

Consent for publication This article does not involve human or animal participation or data, therefore consent to publication is not applicable.

Competing interests The authors declare no competing interests.

Materials availability All material used in this paper are available.

Code availability All codes used in this paper are available.

References

1. Grum J (2002) Induction hardening. In: Handbook of residual stress and deformation of steel, vol 2, pp 220–247
2. Rudnev V, Loveless D, Cook RL (2017) Handbook of induction heating. CRC press
3. Khalifa M (2019) Étude du profil de dureté et de l'effet de bord des disques et engrenages droits traités thermiquement par induction en utilisant les concentrateurs de flux: prédiction et optimisation numérique et expérimentale. Université du Québec à Rimouski
4. Rudnev V (2004) Spin Hardening of Gears Revisited. Heat Treating Progress:17–20
5. Barka N, Bocher P, Brousseau J (2013) Sensitivity study of hardness profile of 4340 specimen heated by induction process using axisymmetric modeling. The International Journal of Advanced Manufacturing Technology 69(9–12):2747–2756
6. Iron GC (1998) Metals Handbook Desk Edition, JR Davis, Editor, pp 309–314
7. Fisk M, Lindgren L-E, Datchary W, Deshmukh V (2018) Modelling of induction hardening in low alloy steels. Finite elements in analysis and design 144:61–75
8. Rajan T, Sharma C, Sharma A (2011) Heat treatment: Principles and techniques. PHI Learning Pvt. Ltd.
9. Putatunda SK (2003) Influence of austempering temperature on microstructure and fracture toughness of a high-carbon, high-silicon and high-manganese cast steel. Materials & design 24(6): 435–443
10. Callister WD, Morin A (2001) Science et génie des matériaux. Dunod
11. Doyon G, Rudnev V, Russell C, Maher J (2017) Revolution-not evolution-necessary to advance induction heat treating. ADVANCED MATERIALS & PROCESSES 175(6):72–80
12. Barka N, Chebak A, El Ouafi A, Jahazi M, Menou A (2014) A new approach in optimizing the induction heating process using flux concentrators: application to 4340 steel spur gear. Journal of materials engineering and performance 23(9):3092–3099
13. Savaria V, Bridier F, Bocher P (2016) Predicting the effects of material properties gradient and residual stresses on the bending fatigue strength of induction hardened aeronautical gears. International Journal of Fatigue 85:70–84
14. Rao S, McPherson D (2003) Experimental characterization of bending fatigue strength in gear teeth. Gear Technol 20(1):25–32

15. FUJITA K, YOSHIDA A, AKAMATSU K (1979) A study on strength and failure of induction-hardened chromium-molybdenum steel spur gears. *Bulletin of JSME* 22(164):242–248
16. Li Z, Ferguson BL Induction hardening process with preheat to eliminate cracking and improve quality of a large part with various wall thickness. In: *International Manufacturing Science and Engineering Conference, 2017*, vol. 50725. American Society of Mechanical Engineers, p V001T02A026
17. Barglik J (2018) Identification of temperature and hardness distribution during dual frequency induction hardening of gear wheels. *Archives of Electrical Engineering*:913–923
18. Kristoffersen H, Vomacka P (2001) Influence of process parameters for induction hardening on residual stresses. *Materials & Design* 22(8):637–644
19. Cajner F, Smoljan B, Landek D (2004) Computer simulation of induction hardening. *J Mater Process Technol* 157:55–60
20. Coupard D, Palin-luc T, Bristiel P, Ji V, Dumas C (2008) Residual stresses in surface induction hardening of steels: comparison between experiment and simulation. *Materials Science and Engineering: A* 487(1-2):328–339
21. Candeo A, Ducassy C, Bocher P, Dughiero F (2011) Multiphysics modeling of induction hardening of ring gears for the aerospace industry. *IEEE Transactions on Magnetics* 47(5):918–921
22. Munikamal T, Sundarraj S (2013) Modeling the case hardening of automotive components. *Metallurgical and Materials Transactions B* 44(2):436–446
23. Montalvo-Urquiza J, Liu Q, Schmidt A (2013) Simulation of quenching involved in induction hardening including mechanical effects. *Computational Materials Science* 79:639–649
24. Barglik J, Smalcerz A, Przulucki R, Doležel I (2014) 3D modeling of induction hardening of gear wheels. *Journal of Computational and Applied Mathematics* 270:231–240
25. Gao K, Qin X, Wang Z, Chen H, Zhu S, Liu Y, Song Y (2014) Numerical and experimental analysis of 3D spot induction hardening of AISI 1045 steel. *Journal of Materials Processing Technology* 214(11):2425–2433
26. Ivanov D, Asperheim JI, Markegård L (2015) Residual stress distribution in induction hardened gear. In: *28th ASM Heat treating society conference*, pp 29–34
27. Chovan J, Slodička M (2017) Induction hardening of steel with restrained Joule heating and nonlinear law for magnetic induction field: Solvability. *Journal of Computational and Applied Mathematics* 311:630–644
28. Hömberg D, Liu Q, Montalvo-Urquiza J, Nadolski D, Petzold T, Schmidt A, Schulz A (2016) Simulation of multi-frequency-induction-hardening including phase transitions and mechanical effects. *Finite Elements in Analysis and Design* 121:86–100
29. Gao K, Wang Z, Qin X-p, Zhu S-x (2016) Numerical analysis of 3D spot continual induction hardening on curved surface of AISI 1045 steel. *Journal of Central South University* 23(5):1152–1162
30. Tawa H (2020) Method for manufacturing gear. ed: Google Patents
31. Zhao Y-Q, Han Y, Xiao Y (2020) An asynchronous dual-frequency induction heating process for bevel gears. *Applied Thermal Engineering* 169:114981
32. Wen H, Han Y, Zhang X, Liu F, Zhang H (2021) Study on electromagnetic heating process of wind power gear: temperature morphology and evolution. *Journal of Thermal Science and Engineering Applications* 13(3)
33. Barglik J, Golak S, Smalcerz A, Wieczorek T (2019) Numerical modeling of induction hardening of gear wheels made of steel AMS 6419. *Metalurgija* 58(1-2):143–146
34. Baldan M, Nikanorov A, Nacke B (2019) A parallel multi-fidelity optimization approach in induction hardening. *COMPEL-The international journal for computation and mathematics in electrical and electronic engineering*
35. Li H, Zhou W, Liu H, Li Z, He L (2019) Analysis of phase transformation and mechanical properties of 55CrMo steel during induction hardening. *Journal of Testing and Evaluation* 49(1)
36. Han Y, Yu E-L, Zhao T-X (2016) Three-dimensional analysis of medium-frequency induction heating of steel pipes subject to motion factor. *International Journal of Heat and Mass Transfer* 101: 452–460
37. Fu X, Wang B, Zhu X, Tang X, Ji H (2017) Numerical and experimental investigations on large-diameter gear rolling with local induction heating process. *The International Journal of Advanced Manufacturing Technology* 91(1-4):1–11
38. Tong D, Gu J, Totten GE (2018) Numerical investigation of asynchronous dual-frequency induction hardening of spur gear. *International Journal of Mechanical Sciences* 142:1–9
39. Barka N, Chebak A, Ouafi AE, Bocher P, Brousseau J (2012) Sensitivity study of temperature profile of 4340 spur gear heated by induction process using 3D model. In: *Applied Mechanics and Materials*, vol 232. Trans Tech Publ, pp 736–741
40. Barka N (2017) Study of the machine parameters effects on the case depths of 4340 spur gear heated by induction—2D model. *The International Journal of Advanced Manufacturing Technology* 93(1-4):1173–1181
41. Khalifa M, Barka N, Brousseau J, Bocher P (2019) Reduction of edge effect using response surface methodology and artificial neural network modeling of a spur gear treated by induction with flux concentrators. *The International Journal of Advanced Manufacturing Technology*:1–15
42. Khalifa M, Barka N, Brousseau J, Bocher P (2019) Optimization of the edge effect of 4340 steel specimen heated by induction process with flux concentrators using finite element axis-symmetric simulation and experimental validation. *The International Journal of Advanced Manufacturing Technology* 104(9-12):4549–4557
43. G. Taguchi, “Introduction to quality engineering: designing quality into products and processes.” 1986.
44. M. J. Crawley, *Statistical computing an introduction to data analysis using S-Plus* (no. 001.6424 C73). 2002.
45. Chandler H (1994) *Heat treater’s guide: practices and procedures for irons and steels*. ASM international
46. Jamil W et al (2016) Mechanical properties and microstructures of steel panels for laminated composites in armoured vehicles. *International Journal of Automotive & Mechanical Engineering* 13(3)
47. Khalifa M, Barka N, Brousseau J, Bocher P (2019) Sensitivity study of hardness profile of 4340 steel disc hardened by induction according to machine parameters and geometrical factors. *The International Journal of Advanced Manufacturing Technology* 101(1-4):209–221
48. Berk J, Berk S (2000) *Quality management for the technology sector*. Elsevier
49. Taguchi G (1993) *Taguchi on robust technology development. bringing quality engineering upstream*. ed: ASME Press, New York
50. Roy RK (2010) *A primer on the Taguchi method*. Society of Manufacturing Engineers
51. Karganroudi SS, Kemda VBF, Barka N (2020) A novel method of identifying porosity during laser welding of galvanized steels using microhardness pattern matrix. *Manufacturing Letters* 25:98–101
52. Barka N, Sattarpanah Karganroudi S, Fakir R, Thibeault P, Feujofack Kemda VB (2020) Effects of laser hardening process

- parameters on hardness profile of 4340 steel spline—an experimental approach. *Coatings* 10(4):342
53. Montgomery DC, Runger GC, Hubele NF (2009) *Engineering statistics*. John Wiley & Sons
 54. Fowlkes WY, Creveling CM (1995) *Engineering methods for robust product design: using Taguchi methods in technology and product development*. Addison-Wesley
 55. Montgomery DC (2001) *Design and analysis of experiments*, vol 1997. John Wiley & Sons, Inc., New York, p 200.1
 56. Grace-Martin SASK (2010) *Data analysis with SPSS: a first course in applied statistics*. *Statistics* 4:27
 57. Frost J (2019) *Regression analysis. An intuitive guide for using and interpreting linear models*. ebook

Publisher's note Springer Nature remains neutral with regard to jurisdictional claims in published maps and institutional affiliations.